Monthly Notices
of the
ROYAL ASTRONOMICAL SOCIETY

Mon. Not. R. Astron. Soc. **407,** 133–143 (2010) doi:10.1111/j.1365-2966.2010.16929.x

Star clusters in the Sh2-132 complex: clues about the connection between embedded and open clusters

T. A. Saurin,★ E. Bica★ and C. Bonatto★

Universidade Federal do Rio Grande do Sul, Departamento de Astronomia, CP 15051, RS, Porto Alegre 91501-970, Brazil

Accepted 2010 April 27. Received 2010 April 26; in original form 2009 December 14

ABSTRACT

Embedded clusters are formed in molecular clouds where massive stars can produce H II regions. The detailed evolutionary connection between embedded and open clusters, and the origin of associations are still to be discovered. There appears to be a high infant mortality rate among embedded clusters, and the few survivors evolve to open clusters. We study the colour–magnitude diagrams (CMDs) and structure of the star clusters related to the Sh2-132 H II region using the Two-Micron All-Sky Survey (2MASS) data base. The fundamental and structural parameters of clusters are determined using main-sequence and pre-main-sequence isochrones and stellar radial density profiles. We report on the discovery of four clusters. One of these is projected a few diameters away from the optical cluster, Teutsch 127, and appears to be deeply embedded, seen only in the infrared. Evidence is found that we are witnessing the dynamical transition from an embedded to an open cluster. An additional cluster is also close to Teutsch 127 and might be associated with a bow-shock. We also study the CMD and structure of the open cluster, Berkeley 94, in Sh2-132, and a new cluster that is projected in the outskirts of the complex. Finally, we have searched for star clusters around the two known Wolf–Rayet stars in the complex. One of these appears to be related to a compact cluster. Finally, the present analyses suggest early dynamical evolution for young star clusters.

Key words: stars: formation – open clusters and associations: individual: Teutsch 127 – open clusters and associations: individual: Berkeley 94.

1 INTRODUCTION

Early star cluster evolution generally leads to dissolution into the field as a result of rapid gas expulsion associated with the evolutionary effects of massive stars, such as supernovae and stellar winds. This causes abrupt changes in the gravitational potential, to the point that significant fractions of the low-mass stars with high velocity in the outer region escape from the cluster (e.g. Tutukov 1978; Fellauer & Kroupa 2005; Bastian & Gieles 2008). Bound open clusters (OCs; i.e. those that keep dynamical stability after the first ∼30–40 Myr) appear to be a minority of about 5 per cent (Lada & Lada 2003). There is a high discrepancy between the birth rate of embedded clusters (2–4 Myr^{-1} kpc^{-2}; Lada & Lada 2003) and OCs (0.25 Myr^{-1} kpc^{-2} according to Elmegreen & Clemens 1985 and 0.45 Myr^{-1} kpc^{-2} according to Battinelli & Capuzzo-Dolcetta 1991) within 2 kpc of the Sun. This is likely a consequence of the high rate of infant mortality. The cluster survival depends primarily on the dynamical state of the stars (i.e. their virial ratio immediately before the onset of gas expulsion; Goodwin 2009), while the star formation efficiency has a secondary role. As an example of a dissolving cluster, a recent study showed that Bochum 1 has an eroded radial density profile (RDP) and a detached core, suggesting, in this case, the genesis of a small OB association (Bica, Bonatto & Dutra 2008).

Young OCs are probes of the early physical processes occurring in embedded and post-embedded clusters. In recent years, our group has analysed main-sequence (MS) and pre-main-sequence (PMS) stellar contents of such objects using powerful tools for field decontamination (NGC 4755 in Bonatto et al. 2006a; NGC 6611 in Bonatto, Santos & Bica 2006b; Pismis 5, NGC 1931, vdB 80 and BDBS 96 in Bonatto & Bica 2009a; and NGC 2244 in Bonatto & Bica 2009b).

The development of infrared astronomy during the last few years has improved our understanding about the origin of clusters, but there are many questions still to be answered. Can all intermediate steps of early cluster evolution be tracked? Can evolutionary scenarios be tested? The present paper, together with other recent papers by our group, address this puzzle, which is fundamental for the understanding of the build-up of star cluster and field populations in the Galaxy.

Another fundamental question is whether massive stars can be formed in isolation, or if isolated massive stars are remnants of

★E-mail: tiago.saurin@ufrgs.br (TAS); bica@if.ufrgs.br (EB);charles@if.ufrgs.br(CB)

Table 1. Known and newly found star clusters in the Sh2-132 area. The columns are: (1) Galactic longitude; (2) Galactic latitude; (3) right ascension (J2000); (4) declination (J2000); (5) radius for decontamination; (6) star cluster name; (7) comments.

l (1)	b (2)	α (3)	δ (4)	r (5)	Name (6)	Comments (7)
102.°81	−0.°67	$22^h19^m00\overset{s}{.}0$	56°07′25.″0	1.′5	Teutsch 127[a]	Optical embedded open cluster, includes Trap 900
102.°81	−0.°71	$22^h19^m08\overset{s}{.}2$	56°05′17.″5	0.′4	SBB 1	Infrared embedded cluster with IRAS 22172+5549
102.°78	−0.°70	$22^h18^m56\overset{s}{.}7$	56°05′10.″9	0.′5	SBB 2	Optical embedded cluster with bow-shock
103.°13	−1.°18	$22^h22^m54\overset{s}{.}3$	55°52′24.″0	2.′0	Berkeley 94[a]	Optical open cluster on the outskirts of the complex
102.°23	−0.°86	$22^h16^m24\overset{s}{.}1$	55°37′37.″0	0.′8	SBB 3	Compact optical open cluster surrounding WR 152
103.°58	−0.°60	$22^h23^m24\overset{s}{.}3$	56°36′27.″0	1.′5	SBB 4	Optical open cluster on the outskirts of the complex

[a]From the SIMBAD data base.

dispersed embedded clusters. de Wit et al. (2004) and de Wit et al. (2005) found that 4 ± 2 per cent of all O-type stars with $V < 8$ mag could have been formed outside a cluster. Parker & Goodwin (2007) have suggested that some apparently isolated O stars are in fact low-mass clusters (<100 $M_\odot$) with only one massive star. *N*-body simulations by Pflamm-Altenburg & Kroupa (2006) showed that the Orion Nebula cluster could have lost at least half of its OB stars as runaways during early cluster evolution. The presence of bow-shocks associated with massive stars can be used as an indicator of ejection of these stars at supersonic velocities (e.g. Gvaramadze & Bomans 2008), when the proper motion cannot be measured properly because of large distances and shortly separated epochs. However, only a fraction, $\lesssim$20 per cent, of runaway OB stars produce bow-shocks.

In the present study, we explore a star-forming complex related to the Sh2-132 H II region (Sharpless 1959) that embeds some previously undetected clusters. Using Two-Micron All-Sky Survey (2MASS[1]) photometry, we analyse the colour–magnitude diagrams (CMDs) and RDPs of five star clusters related to or possibly related to Sh2-132 H II. An additional star cluster projected close to the complex is also studied. A radio continuum emission analysis of Sh2-132 (Harten, Felli & Tofani 1978) indicated the giant nature of this complex and its evolved character (low electron densities, large linear diameter and an ionized gas mass greater than $10^4 M_\odot$), which suggests a suitable laboratory for early dynamical and hydrodynamical evolution.

We also investigate two Wolf–Rayet (WR) stars in the area, searching for possible star clusters around them.

In Section 2 we present the targets. In Section 3, we carry out CMD analysis and estimate cluster parameters. In Section 4 we study the density profiles. Discussions are given in Section 5. Finally, the conclusions of this work are in Section 6.

2 NEWLY FOUND AND PREVIOUSLY KNOWN STAR CLUSTERS

The number of embedded star clusters in a given star-forming region is essential to study the gas expulsion and dynamical evolution effects, in order to know about cluster binarity or multiplicity (Carvalho et al. 2008). In this area of the investigation, we searched for new embedded clusters in the Sh2-132 complex.

We present in Table 1 the star clusters in the area of Sh2-132. The radii given in column 5 were chosen by eye for decontamination purposes (Section 3), as they provide a good contrast with the field. Fig. 1 shows an *R*-band Digitalized Sky Survey (XDSS[2]) image of the whole complex with the positions of the star clusters (Table 1) together with the dark nebulae LDN 1150, LDN 1154 and LDN 1161 (Lynds 1962). SBB 1, SBB 2, SBB 3 and SBB 4 were found by one of us (TAS) using the 2MASS Atlas. The optical OC Teutsch 127 (Kronberger et al. 2006) contains a trapezium system (Trap 900) found by Abt & Corbally (2000). Berkeley 94 was studied with photographic photometry by Yilmaz (1970) and the derived parameters are given in WEBDA[3]: age t = 10 Myr, reddening $E(B–V) = 0.61$ and distance from the Sun $d_\odot = 2.63$ kpc. It is important to analyse Berkeley 94 also with 2MASS photometry for comparison purposes.

The Sh2-132 complex includes two WR stars (van der Hucht 2001; see also the VizieR[4] catalogue III/215). We list in Table 2 their basic properties. These were indicated as members of the Sh2-132 complex and the OB association Cep OB1. Cappa et al. (2008) analysed the distribution of interstellar matter in the neighbourhood of WR 152 and WR 153ab with radio and optical data. They found an H I bubble surrounding the ionized shell of WR 152 and the occurrence of photodissociation at the interface between the ionized and molecular gas around WR 153ab.

For the known OCs (Teutsch 127 and Berkeley 94) SIMBAD[5] lists some early-type stars (Table 3) with their positions, spectral types and *V* magnitudes. We indicate the related clusters in the last column of Table 3.

Fig. 2 shows an XDSS *R*-band image containing the embedded star clusters, Teutsch 127, SBB 1, and SBB 2, together with the WR 153ab star. SBB 1 and Teutsch 127 are very similar in the 2MASS bands. However, SBB 1 becomes invisible in the *B* band of the DSS. This has led us to refer to SBB 1 and Teutsch 127 as 'twins of different colours'. Figs 3 and 4 show enlarged 2MASS images in the K_s band of the embedded infrared cluster SBB 1 and the embedded optical cluster SBB 2, respectively. Fig. 5 shows an XDSS *R*-band image of the faint compact star cluster SBB 3 surrounding the WR 152 star. Fig. 6 shows an XDSS *R*-band image of the star cluster SBB 4 on the outskirts of Sh2-132. Images of Berkeley 94 can be found in WEBDA and XDSS.

3 CMD ANALYSIS

3.1 CMD construction

Photometry in the 2MASS *J*, *H* and K_s bands was extracted in circular fields of radius 40 arcmin with VizieR[6] catalogue II/246, centred on the coordinates listed in Table 1. As a quality constraint,

[1] http://www.ipac.caltech.edu/2mass
[2] http://www1.cadc-ccda.hia-iha.nrc-cnrc.gc.ca/cadc
[3] http://www.univie.ac.at/webda/webda.html
[4] http://vizier.u-strasbg.fr/viz-bin/VizieR?-source=III/215
[5] http://simbad.u-strasbg.fr/simbad
[6] http://vizier.u-strasbg.fr/viz-bin/VizieR?-source=II/246

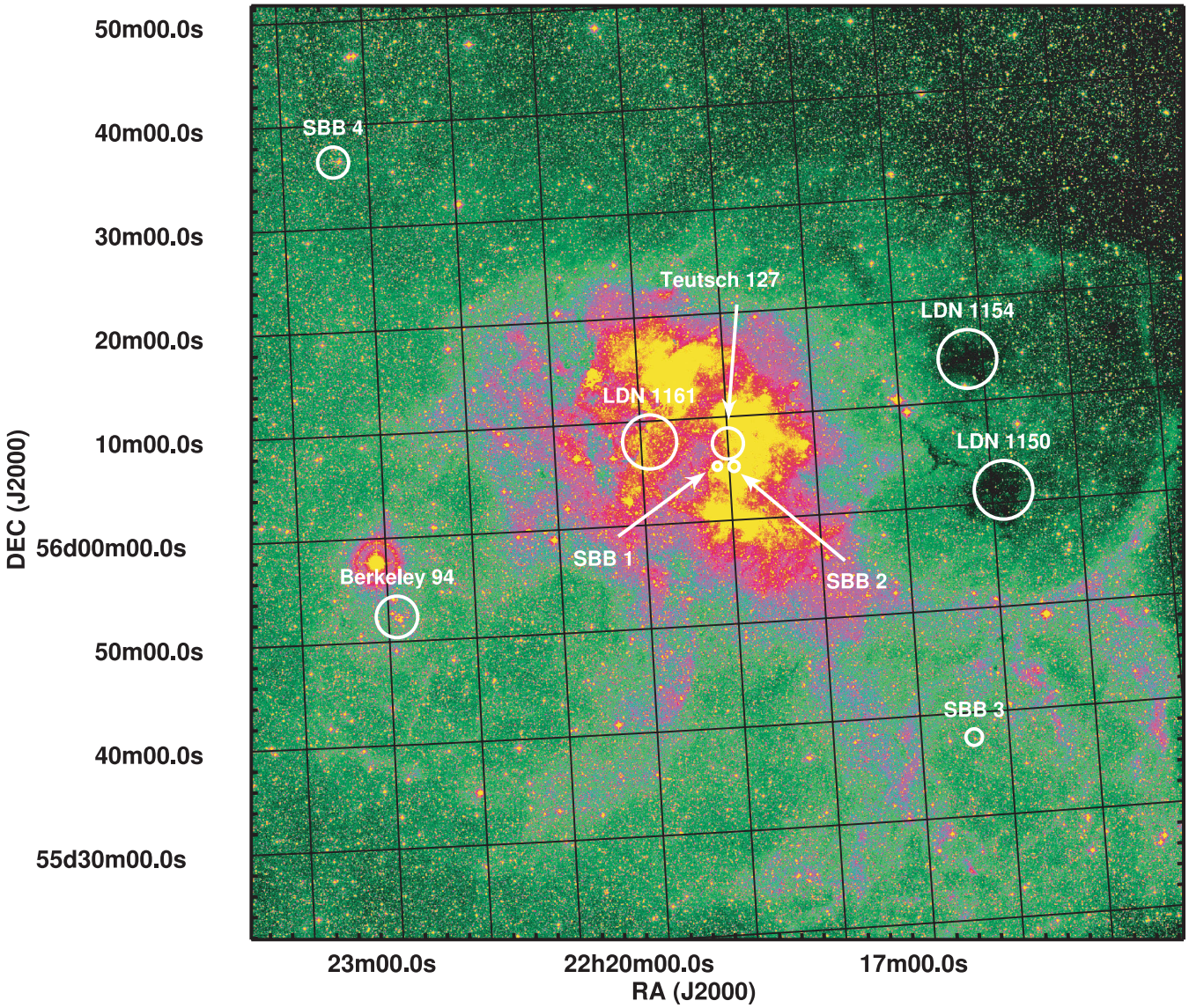

Figure 1. XDSS *R*-band image in false colours of Sh2-132 with all star clusters of the present study (circle radii are listed in Table 1). Dark nebulae in the area are indicated by circle radii 2.83 arcmin for LDN 1150 and LDN 1154, and 2.62 arcmin for LDN 1161 (Lynds 1962). A large bubble appears to be related to the cluster Berkeley 94, and another encloses the dark nebulae LDN 1150 and LDN 1154.

Table 2. WR stars in Sh2-132 (van der Hucht 2001). The columns are: (1) Wolf–Rayet star name; (2) right ascension (J2000); (3) declination (J2000); (4) *V*-band absorption; (5) distance from the Sun; (6) spectral type (Hamann et al. 2006; Smith et al. 1996); (7) association; (8) H II region.

Name (1)	α (2)	δ (3)	A_V (4)	d (kpc) (5)	ST (6)	Association (7)	H II region (8)
WR 152, HD 211564	$22^h16^m24\overset{s}{.}1$	$55^\circ37'37''$	1.62	2.75	WN3(h)-w	Cep OB1	Sh2-132
WR 153ab, HD 211853	$22^h18^m45\overset{s}{.}6$	$56^\circ07'37''$	2.28	2.75	WN6o+O6 I	Cep OB1	Sh2-132

we only considered stars with photometric errors $\leq$0.1 mag in every band.

CMDs displaying $J \times (J–H)$ and $J \times (J–K_s)$ for the cluster stellar content and field stars for equal area (note that the decontamination itself is based on larger fields to improve statistics) as the clusters are shown in Figs 7–12.

As proper motions are not available for a statistically significant sample of stars in the target area, the field star decontamination approach used in this work is based essentially on photometric properties. Given a spatial extraction where a cluster is supposed to exist, and a comparison field (usually large enough to provide statistical representativity in terms of colours and magnitude; e.g. Bonatto & Bica 2009b), the method compares the density of stars, within equivalent CMD cells, in both regions. To take full advantage of the 2MASS photometry, the geometry of the CMD cells is three-dimensional, with axes along J, $(J–H)$ and $(J–K_s)$. The size step

Table 3. Early-type stars in the area of the clusters (SIMBAD). The columns are: (1) early-type star name; (2) right ascension (J2000); (3) declination (J2000); (4) spectral type; (5) absolute magnitude in V band; (6) related cluster.

Name (1)	α (2)	δ (3)	ST (4)	V (5)	Related Cluster (6)
BD+55 2722[a]	$22^h18^m59\overset{s}{.}1$	$56°07'23''$	O9V	9.54	Teutsch 127
TYC 3986-3487-1	$22^h18^m59\overset{s}{.}9$	$56°07'19''$	B	10.60	Teutsch 127
BD+55 2736	$22^h22^m52\overset{s}{.}7$	$55°52'13''$	B	9.67	Berkeley 94
TYC 3986-545-1	$22^h22^m51\overset{s}{.}7$	$55°52'31''$	B	11.59	Berkeley 94
TYC 3986-1890-1	$22^h22^m57\overset{s}{.}6$	$55°52'51''$	B	10.22	Berkeley 94
TYC 3986-695-1	$22^h22^m47\overset{s}{.}8$	$55°52'26''$	B5	12.28	Berkeley 94
TYC 3986-1138-1	$22^h22^m50\overset{s}{.}4$	$55°51'38''$	O6	12.14	Berkeley 94

[a]BD+55 2722 is a binary with secondary spectral type unknown (ADS 15834).

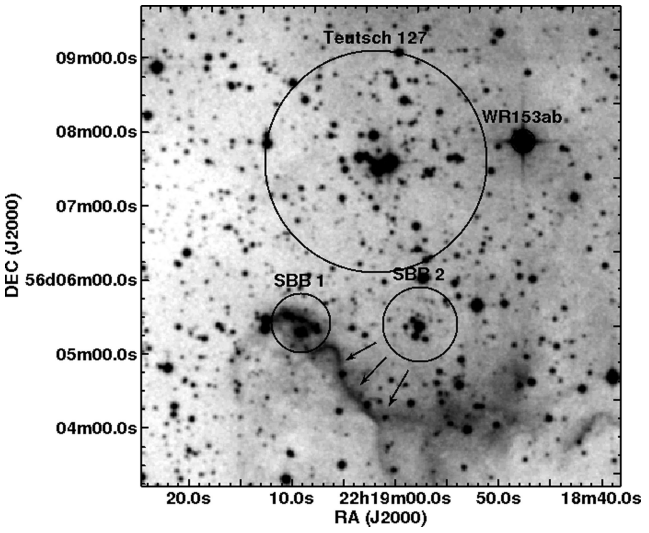

Figure 2. XDSS R-band image of the embedded star clusters in the centre of Sh2-132. The circles with radii listed in Table 1 indicate Teutsch 127, SBB 1 and SBB 2. WR 153ab is the brightest star to the right of Teutsch 127. Arrows indicate a possible bow-shock below SBB 2.

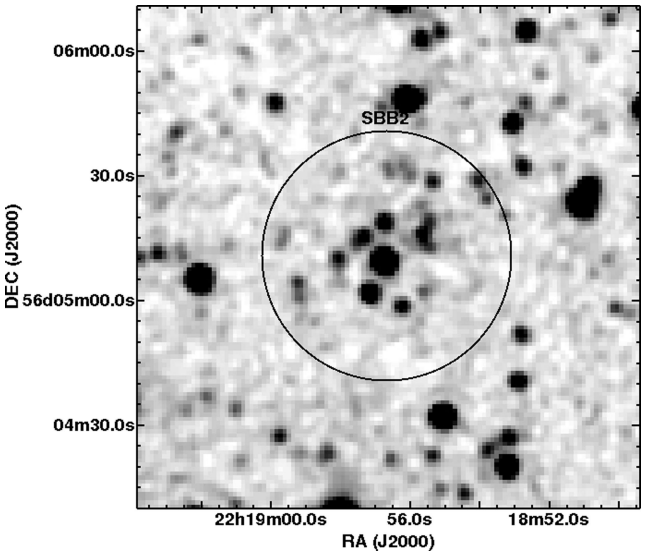

Figure 4. 2MASS K_s-band image of the embedded optical cluster SBB 2. The circle radius is given in Table 1.

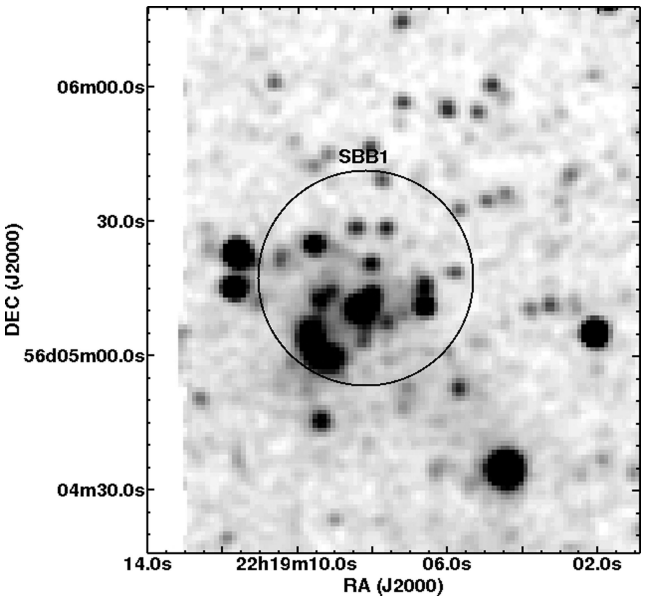

Figure 3. 2MASS K_s-band image of the embedded infrared cluster SBB 1. The circle radius is given in Table 1.

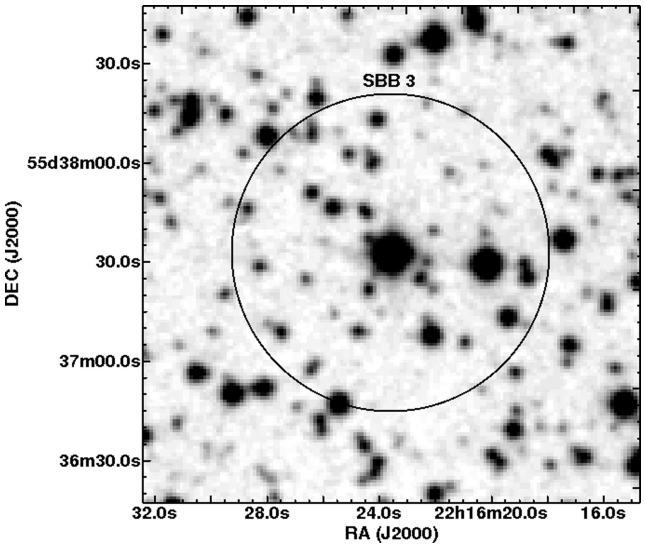

Figure 5. XDSS R-band image of the star cluster SBB 3 surrounding WR 152. The circle radius is given in Table 1.

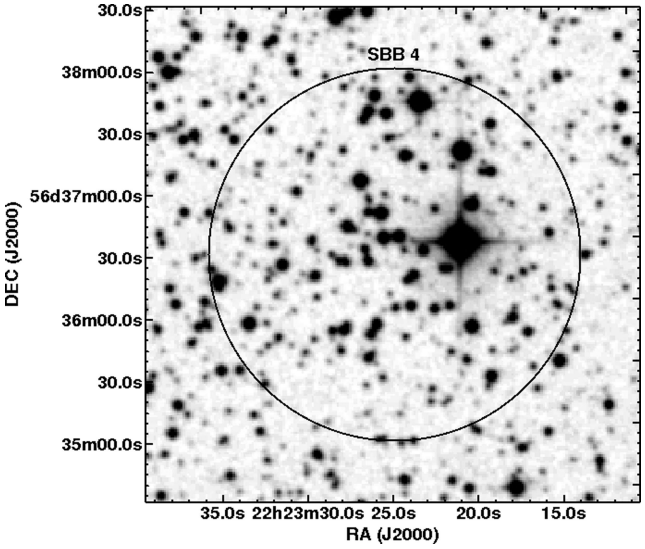

Figure 6. XDSS *R*-band image of the star cluster SBB 4 on the outskirts of Sh2-132. The circle radius is given in Table 1. The brightest star is HD 239944.

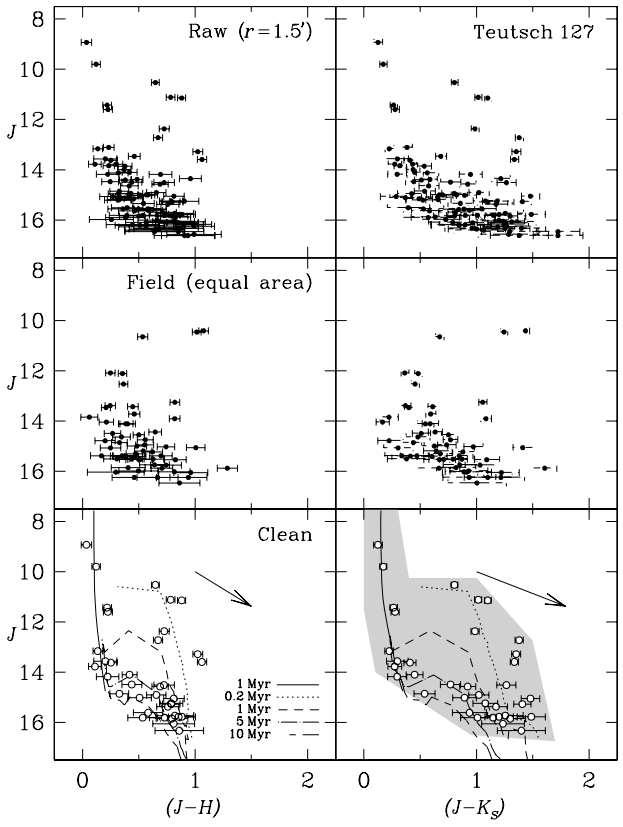

Figure 7. 2MASS CMDs extracted from the $r < 1.5$ arcmin region of Teutsch 127. Top panels: observed photometry with $J \times (J–H)$ (left) and $J \times (J–K_s)$ (right). Middle: equal-area ($29.962 < r < 30$) arcmin extraction from the comparison field. Bottom panels: decontaminated CMDs fitted with 1 Myr Solar metallicity Padova isochrone (Marigo et al. 2008) and 0.2, 1, 5 and 10 Myr PMS isochrones (Siess et al. 2000). The shaded area corresponds to the colour–magnitude filter. The arrows indicate the reddening vectors for $A_V = 5$.

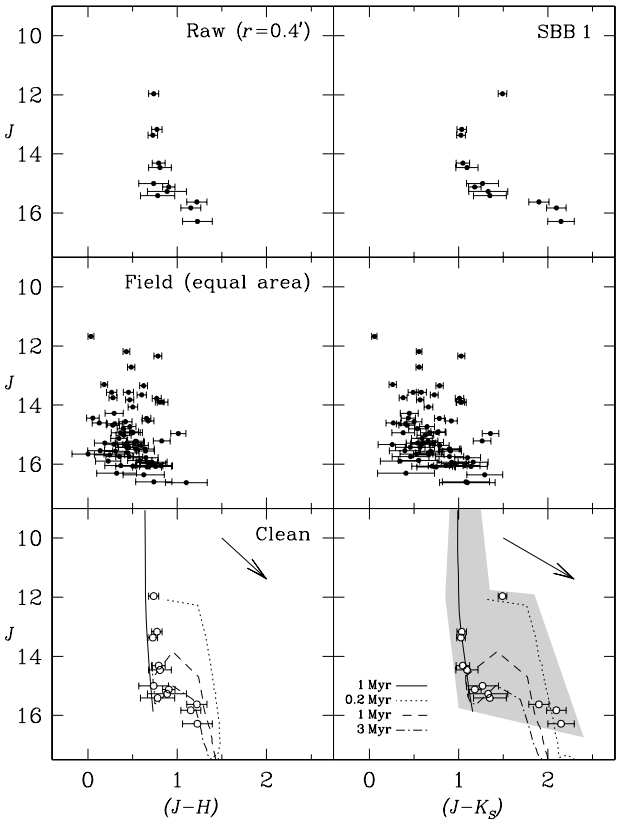

Figure 8. Same as Fig. 7 for the region $r < 0.4$ arcmin of SBB 1 and comparison field between $29.997 < r < 30$ arcmin. PMS isochrones are 0.2, 1 and 3 Myr.

along each dimension is $\Delta J = 1.0$ and $\Delta(J–H) = \Delta(J–K_s) = 0.25$. The cluster extraction radius is given in Table 1 and the comparison field range is $r = 20$–40 arcmin. Basically, for each cluster CMD cell we compute an estimate of the field contamination based on the comparison field. Photometric uncertainties are taken into account, in the sense that what we compute is the probability of a given star to be found in a cell (this reduces to the difference of the error function between the borders of the cells). Summing the probability for all stars, the end result of this procedure is the number-density of stars in a given cell. We do this for the cluster and comparison field cells. Next, the comparison field number-density is converted back into an integer number of stars, which is subtracted from the cluster extraction, on a cell-by-cell basis. Thus, the number of member stars in a given cell is $N^{\rm cell}_{\rm clean}$. Allowing for variations in the cell positioning corresponding to 1/3 of the adopted cell size in each dimension, we are left with 27 different set-ups. Each set-up produces a total number of member stars, $N_{\rm mem} = \sum_{\rm cell} N^{\rm cell}_{\rm clean}$, from which we compute the expected total number of member stars $\langle N_{\rm mem} \rangle$ by averaging out $N_{\rm mem}$ over all combinations. Stars are ranked according to the number of times they survive all runs, and only the $\langle N_{\rm mem} \rangle$ highest ranked stars are considered cluster members and transposed to the respective decontaminated CMD (bottom panels of Figs 7–12). The difference between the expected number of field stars (which may be fractional) and the number of stars effectively subtracted (which is integer) from each cell is the subtraction efficiency, which summed over all cells is 93.6 ± 5.0 per cent for Teutsch 127, 26.4 ± 33.3 per cent for SBB 2, 87.1 ± 3.7 per cent for Berkeley 94, 92.1 ± 2.4 per cent for SBB 3 and

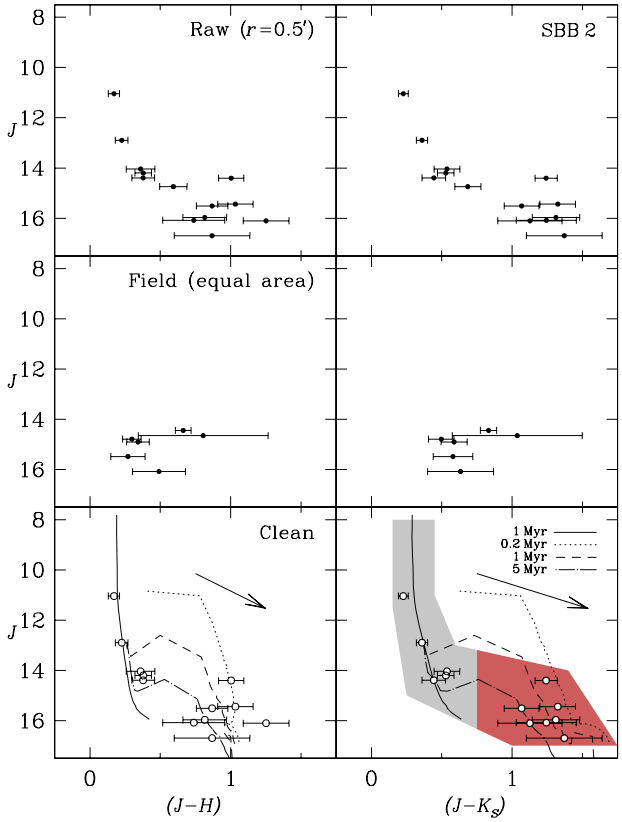

Figure 9. Same as Fig. 7 for the region $r < 0.5$ arcmin of SBB 2 and comparison field between $29.996 < r < 30$ arcmin. PMS isochrones are 0.2, 1 and 5 Myr. The light-shaded polygon is the colour–magnitude filter to isolate the MS stars. The dark-shaded polygon is the colour–magnitude filter for the PMS stars.

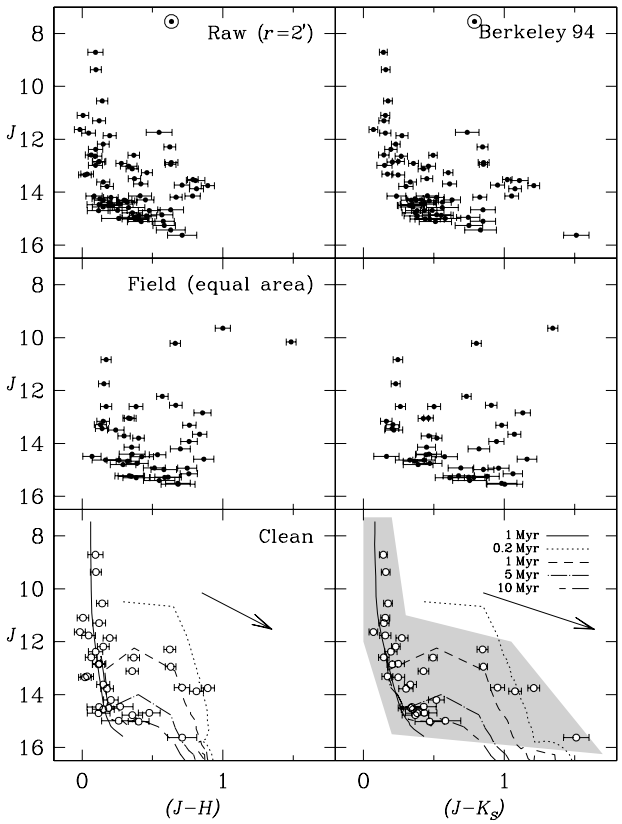

Figure 10. Same as Fig. 7 for the region $r < 2$ arcmin of Berkeley 94 and comparison field between $29.933 < r < 30$ arcmin. PMS isochrones are 0.2, 1, 5 and 10 Myr. Circled points represent the foreground TYC 3986-341-1 star, which is not part of the cluster, although it has been assigned as a member in SIMBAD.

90.9 ± 7.5 per cent for SBB 4. No star has been removed within the area of SBB 1.

All cluster $J \times (J–K_s)$ CMDs of this sample were fitted by eye with 1-Myr Solar metallicity (suitable for the Galactic disc in general) Padova isochrones (Marigo et al. 2008). In addition, PMS isochrones by Siess, Dufour & Forestini (2000) for ages 0.2, 1, 2, 3, 5, 10 and 20 Myr were used when necessary. Isochrone fits for each cluster (Table 4) correspond to a distance from the Sun $d_\odot = 3.6$ kpc (which matches that of Foster & Routledge 2003). This distance locates Sh2-132 in the Orion–Cygnus arm (Momany et al. 2008). Only SBB 4 appears to be closer and is not part of the complex Sh2-132. The isochrone fit for the CMD of this cluster yields a distance from the Sun $d_\odot = 2.27$ kpc.

3.2 CMD results

We detected MS and PMS stars in all clusters, although Teutsch 127 (Fig. 7) and Berkeley 94 (Fig. 10) are more populated. In addition, Teutsch 127 may have a few Herbig Ae/Be stars heading to the MS. These stars are located in the region $(J–K_s) > 0.75$ and $J < 12$ (Fig. 7) in the CMD. The same occurs for SBB 4 (Fig. 12).

The CMDs of Teutsch 127 (Fig. 7), SBB 1 (Fig. 8) and SBB 2 (Fig. 9) show a poorly populated MS, while the CMD of Berkeley 94 (Fig. 10) has a better defined MS. Although each cluster shows PMS stars with ages <10 Myr, SBB 3 has only lower-mass stars ($M < 2$ M$_\odot$) with ages of 10–20 Myr for the PMS. SBB 2 has a detached MS and PMS, and therefore we filtered these separately (Fig. 9).

The star TYC 3986-341-1 is present in SIMBAD as a member of Berkeley 94 and persists after CMD decontamination (Fig. 10), but its spectral type is G8 III, which is incompatible with such a young cluster. The distance modulus derived from the B and V values in SIMBAD reveals that it is very close to the Sun and is not part of the star cluster.

Fig. 13 shows the intrinsic colour–colour diagrams $(H–K_s) \times (J–H)$ for the clusters in the area of Sh2-132. Reddening values (Table 4) obtained by isochrone fits were used to correct the magnitudes with the relations $A_J/A_V = 2.76$, $A_H/A_V = 0.176$, $A_{K_s}/A_V = 0.118$ and $A_J = 2.76\,E(J–H)$ given by Dutra, Santiago & Bica (2002), for $R_V = 3.1$. A comparison with the classical T Tauri star (CTTS) locus (dashed line) obtained by Meyer, Calvet & Hillenbrand (1997) shows that only a few of the PMS stars of our sample are T Tauri stars. Another comparison of the colour–colour diagram with the standard sequence for dwarf stars from Bessel & Brett (1988) reveals the presence of some dwarfs in all clusters, especially Berkeley 94, Teutsch 127 and SBB 4.

The excess in $(H–K_s)$ observed in the colour–colour diagrams for some stars (Fig. 13) suggests circumstellar discs, which characterize many CTTSs (Furlan et al. 2009). These discs dissipate at ∼10 Myr as these stars evolve to weak-lined T Tauri stars and giant planet formation comes to an end.

A comparison of the CMD of Teutsch 127, taking into account absorption and distances, with a PMS template (Fig. 14) built with

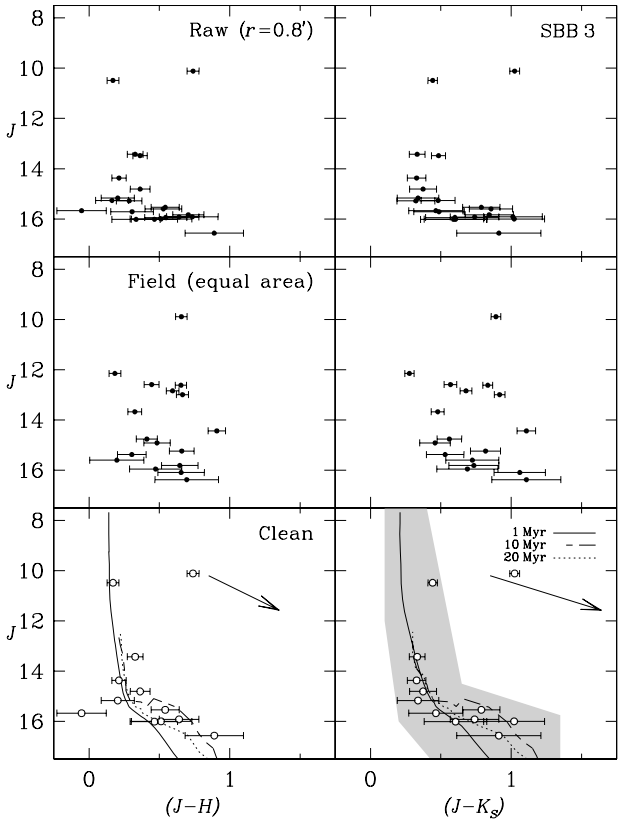

Figure 11. Same as Fig. 7 for the region $r < 0.8$ arcmin of SBB 3 and comparison field between $29.989 < r < 30$ arcmin. PMS isochrones are 10 and 20 Myr.

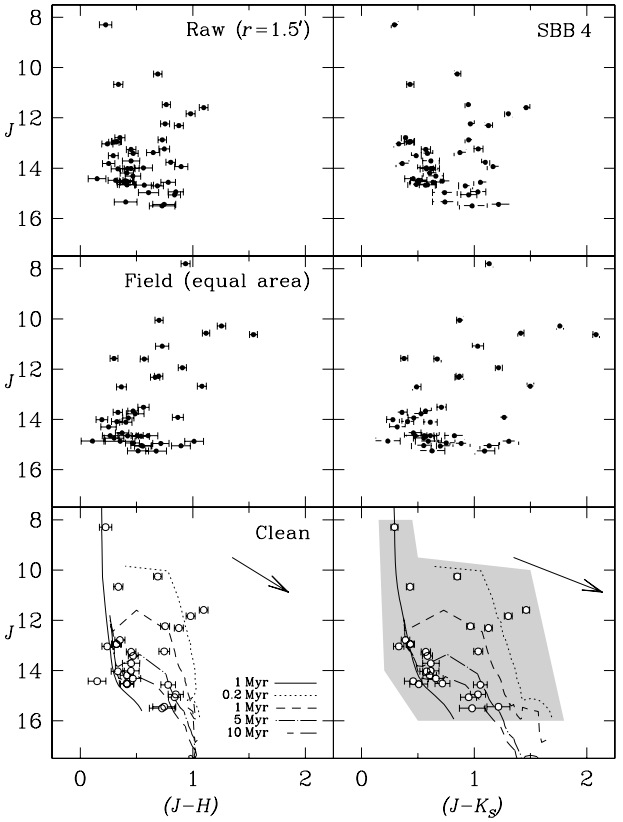

Figure 12. Same as Fig. 7 for the region $r < 1.5$ arcmin of SBB 4 and comparison field between $29.962 < r < 30$ arcmin. PMS isochrones are 0.2, 1, 5 and 10 Myr.

spectral types, magnitudes and colours of the stellar content of Chamaleon I (Luhman 2007, 2008, and references therein) reveals that in Teutsch 127, PMS stars appear to be distributed between B6 (earliest) and M4 (latest), while in SBB 2 they are bracketed by G5 and M4. In the other clusters, this distribution is more restricted. We identify (i) a B6 and a G5 in SBB 1, (ii) F0, G8 and K3 types in SBB 3 and (iii) F0, G8 and K3 types in SBB 4. The M4 lower limit is a result of the observational cut-off.

3.3 CMD spread sources

Open-cluster CMDs can have a broader than usual MS because of several factors, such as photometric errors, binarity variability, field contamination and (most important in the case of embbeded clusters) differential reddening. These effects can disturb isochrone fits. Photometric uncertainty is a function of magnitude, so faint stars (such as PMS) have larger errors (Bonatto & Bica 2007).

A large fraction of stars in clusters appear to be binary, so that points in the CMD are shifted only above the isochrone, unlike other effects (photometric errors and variability). Platais et al. (2007) found a binary fraction of 30 per cent for IC 2391, which has an age of 35 Myr. Converse & Stahler (2008) estimate in 76 per cent the binary fraction in the Pleiades with an age of 125 Myr. However, it is not yet clear whether the reason for differences in the binary fraction among clusters is age or density. Furthermore, tidal stripping tears preferentially low-mass stars from the edge of clusters, so that the binary fraction should increase, unless destruction of binaries occurs.

Some PMS stars of these clusters may be T Tauri and therefore have variable brightness, causing a spread of the points in the CMD. However, only a few T Tauri stars are detectable with 2MASS in the present sample (Section 3.2) because of the large distance of Sh2-132 (Fig. 13).

Differential reddening is the most important factor in the case of star clusters located in regions with large quantities of gas and dust. There is a remarkable large bubble centred close to the dark nebulae LDN 1150 and LDN 1154 to the north-east of Sh2-132 (Fig. 1). In fact, reddening is larger in this direction according to the values (Table 5) derived from the maps of the dust infrared emission of Schlegel, Finkbeiner & Davis (1998). To the west of Teutsch 127 is the dark nebula LDN 1161 (Fig. 1).

These factors act cumulatively on the observed stellar magnitudes scattering the points in the CMDs, but the PMS age spread appears to be a major source of dispersion (Figs 7–12).

4 STELLAR DENSITY PROFILES

In principle, CMDs of bound and un-bound young star clusters are indistinguishable. Structural differences resulting from early changes in the gravitational potential can show up in the stellar RDPs. We can expect that young clusters with stellar dispersion have irregular RPDs that cannot be fitted by any model based on an isothermal sphere (e.g. King 1962; Wilson 1975; Elson, Fall & Freeman 1987).

RDPs were built for the colour–magnitude filtered photometry (Figs 15–20). Background densities ($\sigma_{\rm bg}$) were measured in the field

Table 4. Fundamental parameters derived for the star clusters. The columns are: (1) star cluster name; (2) colour excess $E(J–H)$; (3) colour excess $E(J–K_s)$; (4) observed distance modulus assuming a distance from the Sun $d_\odot = 3.6$ kpc, except for SBB 4 for which we derived $d_\odot = 2.27$ kpc; (5) V-band absorption; (6) age from the oldest PMS isochrone fit; (7) age from the MS isochrone fit; (8) adopted age.

Name	$E(J–H)$	$E(J–K_s)$	$(m–M)J$	A_V	t_0 (Myr)	t_{MS} (Myr)	t (Myr)
(1)	(2)	(3)	(4)	(5)	(6)	(7)	(8)
Teutsch 127	0.26	0.41	13.50	0.25	10	1	∼5
SBB 1	0.80	1.25	14.99	0.78	3	1	∼1
SBB 2	0.35	0.55	13.75	0.34	5	1	∼2
Berkeley 94	0.22	0.34	13.39	0.22	10	1	∼5
SBB 3	0.30	0.47	13.61	0.29	20	1	∼15
SBB 4	0.35	0.55	12.75	0.34	10	1	∼5

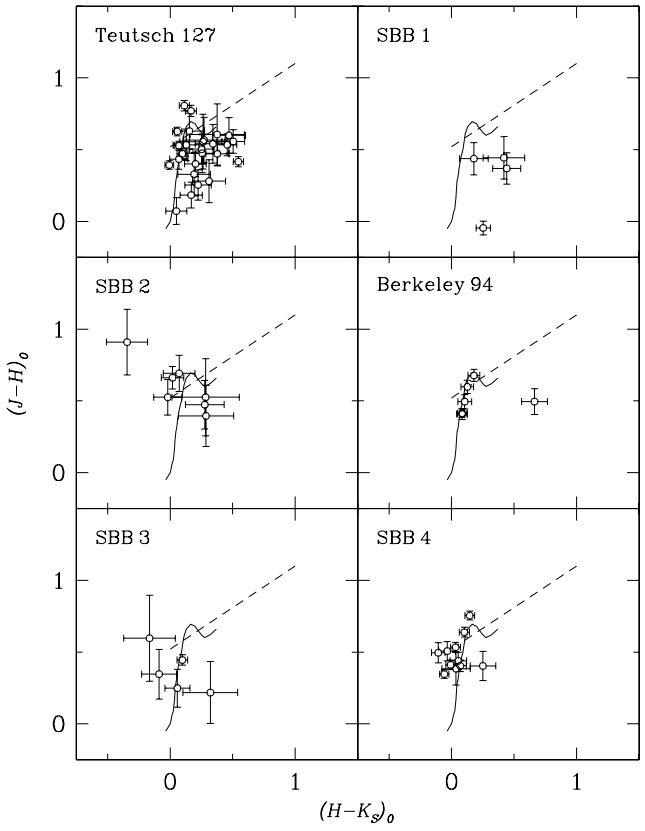

Figure 13. Absolute colour–colour diagrams $(H–K_s) \times (J–H)$ of PMS stars (open circles) of the clusters in the area of Sh2-132. The dashed line is the CTTS locus (Meyer 1997) and the solid line is the dwarf star branch (Bessel & Brett 1988).

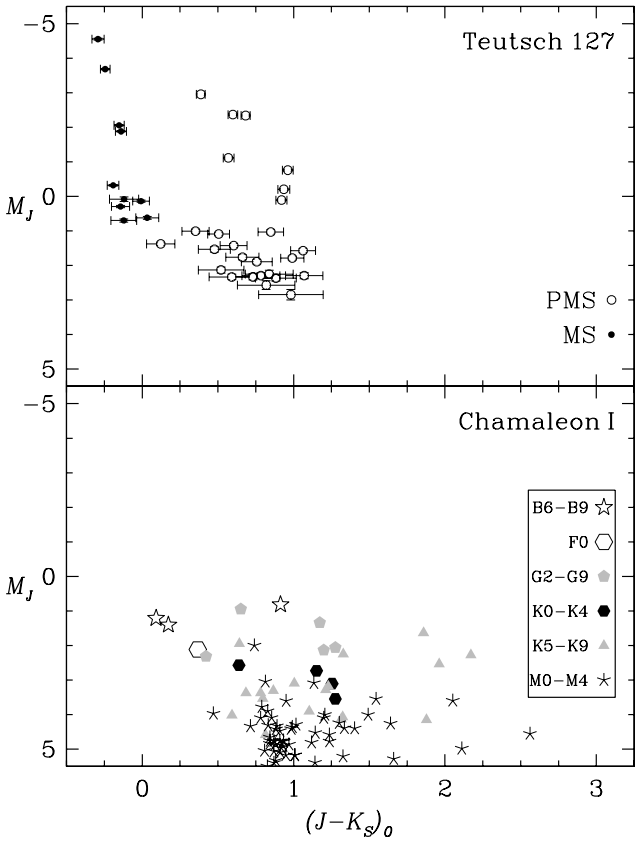

Figure 14. Comparison of the dereddened absolute CMD of Teutsch 127 (top) with the dereddened absolute CMD of a PMS template (bottom) built with data of the stellar content of Chamaleon I (Luhman 2007, 2008).

($r = 20$–40 arcmin). King-like profiles were fitted for the RDPs of Teutsch 127 and Berkeley 94 with a non-linear least-squares routine that uses errors as weights. The structural parameters, central surface density (σ_0) and core radius (r_c), were obtained from this fit, while σ_{bg} was kept constant. The results are shown in Table 6. The RDPs of SBB 1, SBB 2, SBB 3 and SBB 4 could not be fitted by a King-like profile.

The presence of the dark nebula LDN 1161 and its obscuring effect is clearly observed as a depression in the RDP of Teutsch 127 (Fig. 15) for $6 < r < 11$ arcmin.

The RDPs of central clusters (Teutsch 127, SBB 1 and SBB 2) overlap for radii larger than 1 arcmin. These might represent radial profiles of merging clusters (Carvalho et al. 2008).

The RDP of SBB 2 was divided into two components (Fig. 17), one for MS and the other for PMS stars. The total RDP (MS+PMS) is also shown. The higher central density of MS stars may suggest primordial mass segregation with an outer region dominated by lower-mass PMS stars.

The RDP of SBB 3 (Fig. 19) results in a dense and compact core possibly sustained by the gravitational potential of WR 152.

Table 5. Absorptions derived from the maps of dust infrared emission of Schlegel et al. (1998). The columns are: (1) object name; (2) reddening; (3) V-band absorption; (4) J-band absorption.

Object (1)	$E(B-V)$ (2)	A_V (3)	A_J (4)
Teutsch 127	5.888	19.520	5.311
SBB 1	5.361	17.773	4.836
SBB 2	6.100	20.220	5.502
Berkeley 94	0.734	2.433	0.662
SBB 3	1.399	4.638	1.262
SBB 4	0.998	3.310	0.901
LDN 1150	1.283	4.252	1.157
LDN 1154	2.143	7.104	1.933
LDN 1161	3.827	12.686	3.452

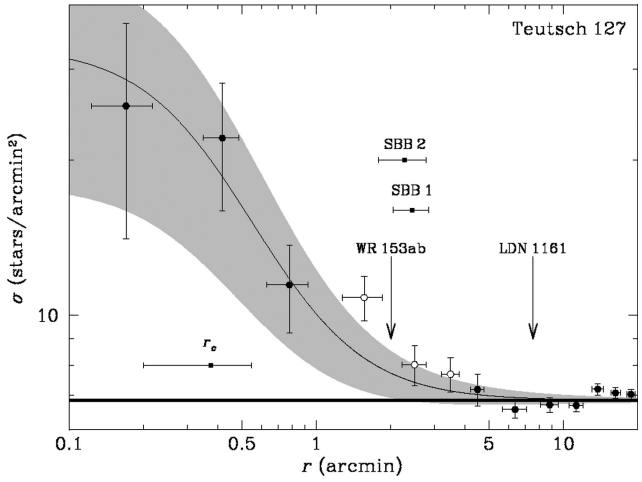

Figure 15. Stellar RDP for Teutsch 127 built with the colour–magnitude filter (Fig. 7). The best-fitting King-like profile is shown as a solid line. Open circles were excluded from the fit. Background stellar level is represented by the shaded stripe in the bottom and the 1σ fit uncertainty is represented by the shaded region along the fit. The core radius (r_c), WR 153ab, SBB 1, SBB 2 and LDN 1161 positions are indicated.

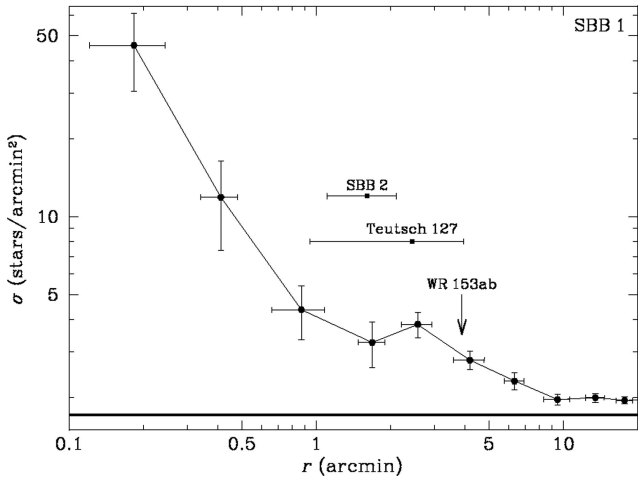

Figure 16. Stellar RDP for SBB 1 built with colour–magnitude photometry. The WR 153ab, SBB 2 and Teutsch 127 positions are indicated.

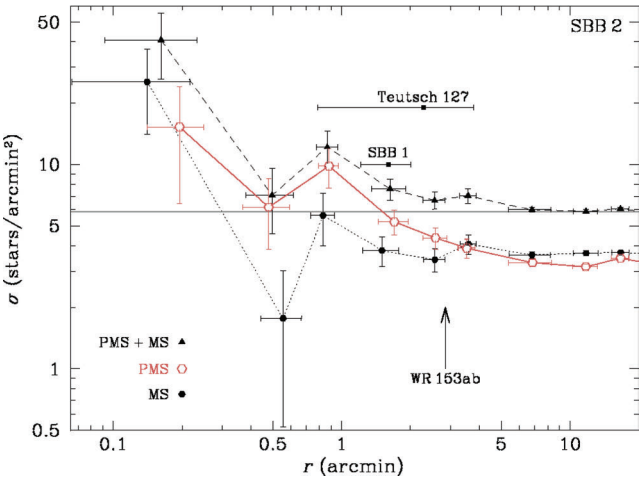

Figure 17. Stellar RDPs for SBB 2 built separately for PMS stars (open circles) and MS (filled circles) stars with colour–magnitude photometry. Stellar RDP of PMS+MS is represented by filled triangles. The WR 153ab, SBB 1 and Teutsch 127 positions are indicated.

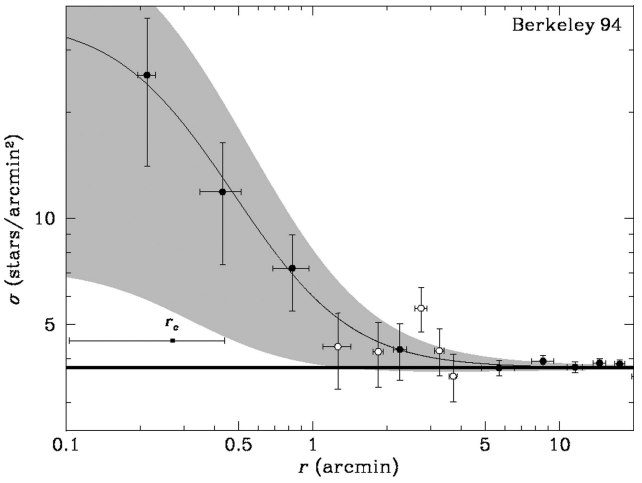

Figure 18. Same as Fig. 15 for Berkeley 94.

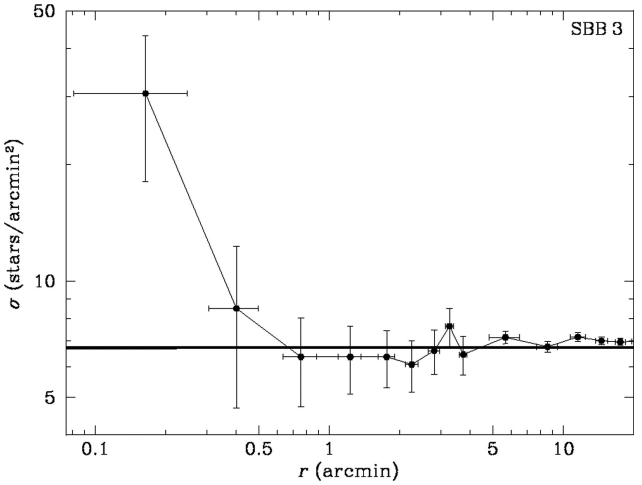

Figure 19. Same as Fig. 16 for SBB 3.

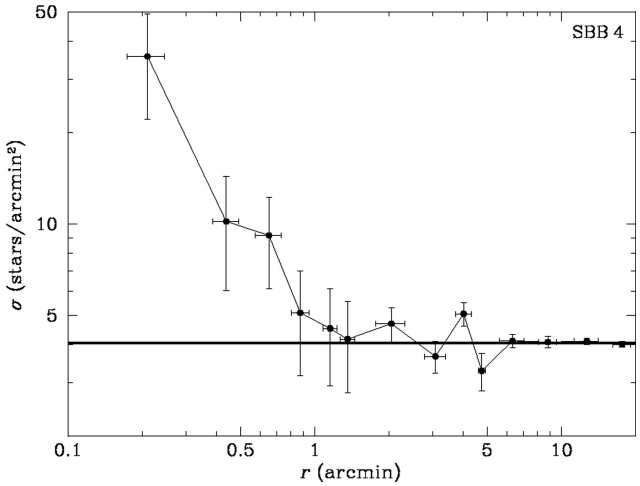

Figure 20. Same as Fig. 16 for SBB 4.

Finally, SBB 4 (Fig. 20) has an irregular RDP with some bumps, which could be evidence of stellar dispersion.

5 DISCUSSION

The morphology of Sh2-132, which contains several bubbles, suggests triggered star formation similar to Sh2-284 (Puga et al. 2009). Additional small star clusters not yet identified are possible in the area of the Sh2-132 complex. A higher-resolution mid-infrared study would be important.

Teutsch 127 appears to be a young OC with age ∼5 Myr, while SBB 1 seems to be ∼1 Myr old. SBB 1 is deeply embedded and may result from a stellar feedback of O- and B-type stars in older surrounding clusters. It is superimposed on a probable bow-shock ∼3 arcmin to the south-west of Teutsch 127 and WR 153ab. However, this bow-shock seems to have been generated in SBB 2. We may be witnessing the sequential effects of star formation.

The presence of the trapezium system, Trap 900, in the centre of Teutsch 127 will certainly have an important role in the cluster evolution. Trapezium systems evolve into hierarchical systems (with a much larger separation among its components) or even disperse in a few million years producing runaway stars. The oldest identified so far has ∼50 Myr (Abt & Corbally 2000).

Teutsch 127 is close to WR 153ab, which is a spectroscopic binary with a primary WN6o and an O6 I (Smith, Shara & Moffat 1996). Evolution of this WR to spectral type WC and its subsequent explosion as a supernova will certainly have an impact on the dynamical evolution of neighbouring clusters (Teutsch 127, SBB 1 and SBB 2), by means of gas removal.

SBB 1 is the youngest cluster in the sample and remains embedded. The residual gas expulsion and stellar evolution may cause an increase of core radius.

As SBB 2 expulsed its residual gas, star formation must have stopped and its survival as a bound OC depends on the dynamics and evolution of neighbouring clusters and especially of the WR 153ab star.

SBB 3 hosts the WR 152 star of type WN3(h)-w, a mass of 12 $M_\odot$ and mass-loss rate $\log \dot{M}(M_\odot yr^{-1}) = -5.5$ (Hamann, Gräfener & Liermann 2006). Because WR 152 has a relatively low mass for a WR star (the minimum initial mass for a star to become a WR at Solar metallicity is 25 $M_\odot$), it can explode as a supernova without evolving through the WC type, expulsing gas and dissolving the star cluster very early.

The following two possible destinations are suggested for the central clusters of Sh2-132.

(i) Given the proximity among these clusters, a merger may occur, which would generate a more massive OC. As a consequence, this cluster would appear dynamically older than the evolution of its stars indicates (i.e. with mass segregation more advanced than expected; Moeckel & Bonnell 2009).

(ii) Alternatively, there may be a dissolution of the clusters, as a consequence of residual gas expulsion, stellar evolution and dynamics of the trapezium system. In this case, Trap 900 might leave a compact fossil remnant.

6 CONCLUDING REMARKS

We report on the discovery of four star clusters (here referred to as SBB 1, SBB 2, SBB 3 and SBB 4) in the area of the Sh2-132 complex. These clusters and two previously catalogued clusters (Teutsch 127 and Berkeley 94) were analysed with 2MASS photometry. These show evidence that the Sh2-132 complex is a site of triggered star formation, as suggested by its hierarchical structure and the age distribution of the star clusters. The presence of gas and dust bubbles reinforces this idea.

ACKNOWLEDGMENTS

We thank an anonymous referee for constructive comments and suggestions. We acknowledge support from the Brazilian Institution CNPq. This publication makes use of data products from the 2MASS, which is a joint project of the University of Massachusetts and the Infrared Processing and Analysis Center/California Institute of Technology, funded by the National Aeronautics and Space

Table 6. Structural parameters of the star clusters. The columns are: (1) star cluster name; (2) central density; (3) core radius (arcmin); (4) core radius (pc) assuming a distance from the Sun $d_\odot = 3.6$ kpc; (5) background density.

Name	σ_0 (star arcmin^{-2})	r_c (arcmin)	r_c (pc)	σ_{bg} (star arcmin^{-2})
(1)	(2)	(3)	(4)	(5)
Teutsch 127	27.05 ± 19.38	0.37 ± 0.21	0.39 ± 0.22	6.39 ± 0.04
SBB 1	–	–	–	1.71 ± 0.02
SBB 2	–	–	–	5.87 ± 0.04
Berkeley 94	32.72 ± 29.23	0.27 ± 0.17	0.28 ± 0.18	3.77 ± 0.03
SBB 3	–	–	–	7.94 ± 0.05
SBB 4	–	–	–	4.05 ± 0.03

Administration and the National Science Foundation. This research has made use of the WEBDA data base, operated at the Institute for Astronomy of the University of Vienna.

REFERENCES

Abt H. A., Corbally C. J., 2000, ApJ, 541, 841
Bastian N., Gieles M., 2008, in de Koter A., Smith L. J., Waters L. B. F. M., eds, ASP Conf. Ser. Vol. 388, Mass Loss from Stars and the Evolution of Stellar Clusters. Astron. Soc Pac., San Francisco, p. 353
Battinelli P., Capuzzo-Dolcetta R., 1991, MNRAS, 249, 76
Bessel M. S., Brett J. M., 1988, PASP, 100, 1134
Bica E., Bonatto C., Dutra C. M., 2008, MNRAS, 489, 1129
Bonatto C., Bica E., 2007, MNRAS, 377, 1301
Bonatto C., Bica E., 2009a, MNRAS, 397, 1915
Bonatto C., Bica E., 2009b, MNRAS, 394, 2127
Bonatto C., Bica E., Ortolani S., Barbuy B., 2006a, A&A, 453, 121
Bonatto C., Santos J. F. C., Jr, Bica E., 2006b, A&A, 445, 567
Cappa C. E., Vasquez J., Arnal E. M., Cichowolski S., Pineault S., 2008, Rev. Mex. Astron. Astrofís. Conf. Ser., 33, 142
Carvalho L., Saurin T. A., Bica E., Bonatto C., Schmidt A., 2008, A&A, 485, 71
Converse J. M., Stahler S. W., 2008, ApJ, 678, 431
de Wit W. J., Testi L., Palla F., Vanzi L., Zinnecker H., 2004, A&A, 435, 937
de Wit W. J., Testi L., Palla F., Zinnecker H., 2005, A&A, 437, 247
Dutra C. M., Santiago B. X., Bica E., 2002, A&A, 381, 219
Elmegreen B. G., Clemens C., 1985, ApJ, 294, 523
Elson R. A. W., Fall S. M., Freeman K. C., 1987, ApJ, 323, 54
Fellhauer M., Kroupa P., 2005, ApJ, 630, 879
Foster T., Routledge D., 2003, ApJ, 598, 1005
Furlan E. et al., 2009, ApJ, 703, 1964
Goodwin S. P., 2009, Ap&SS, 324, 259
Gvaramadze V. V., Bomans D. J., 2008, A&A, 490, 1171
Hamann W.-R., Gräfener G., Liermann A., 2006, A&A, 457, 1015
Harten R. H., Felli M., Tofani G., 1978, A&A, 70, 205
King I., 1962, AJ, 67, 471
Kronberger M. et al., 2006, A&A, 447, 921
Lada C. J., Lada E. A., 2003, ARA&A, 41, 57
Luhman K. L., 2007, ApJS, 173, 104
Luhman K. L., 2008, in Reipurth B., ed., Handbook of Star-Forming Regions, Vol. II: The Southern Sky. Astron. Soc. Pac., San Francisco, p. 169
Lynds B. T., 1962, ApJS, 7, 1
Marigo P., Girardi L., Bressan A., Groenewegen M. A. T., Silva L., Granato G. L., 2008, A&A, 482, 883
Meyer M. R., Calvet N., Hillenbrand L. A., 1997, AJ, 114, 288
Moeckel N., Bonnell I. A., 2009, MNRAS, 400, 657
Momany Y., Ortolani S., Bonatto C., Bica E., Barbuy B., 2008, MNRAS, 391, 1650
Parker R. J., Goodwin S. P., 2007, MNRAS, 380, 1271
Pflamm-Altenburg P., Kroupa J., 2006, MNRAS, 373, 295
Platais I., Melo C., Mermilliod J.-C., Kozhurina-Platais V., Fulbright J. P., Méndez R. A., Altmann M., Sperauskas J., 2007, A&A, 461, 509
Puga E., Hony S., Neiner C., Lenorzer A., Hubert A.-M., Waters L. B. F. M., Cusano F., Ripepi V., 2009, A&A, 503, 107
Schlegel D. J., Finkbeiner D. P., Davis M., 1998, ApJ, 500, 525
Sharpless S., 1959, ApJS, 4, 257
Siess L., Dufour E., Forestini M., 2000, A&A, 358, 593
Smith L. F., Shara M. M., Moffat A. F. J., 1996, MNRAS, 281, 163
Tutukov A. V., 1978, A&A, 70, 57
van der Hucht K. A., 2001, NewAR, 45, 135
Wilson C. P., 1975, AJ, 80, 175
Yilmaz F., 1970, A&A, 8, 213

This paper has been typeset from a TEX/LATEX file prepared by the author.